

Modeling of Terabit Geostationary Terahertz Satellite Links from Globally Dry Locations

Jonathan Y. Suen, *Student Member, IEEE*, Michael T. Fang, Sean P. Denny, and Philip M. Lubin

Abstract—While terahertz communication systems, operating from 100 GHz to 1 THz, have the potential to utilize wide swaths of unused spectrum for ultra-high bitrate communication, there are significant challenges. Particularly, the strong absorption of water vapor can result in very high atmospheric attenuation. We modeled a ground to geostationary satellite link and found that using large aperture THz stations, patterned after the 12.5 m Atacama Large Microwave Array dish and the 3.5 m Herschel Space Observatory optics, worst 10th percentile data rates in excess of one terabit per second in the THz bands are possible. The key is to place ground stations in dry regions. We locate these by coupling our link model, which selects optimum modulation and carrier bandwidth, with global, high-resolution satellite water vapor measurements. We present detailed maps showing modeled link performance over the surface of the Earth. Smaller apertures on aircraft and balloons are also able to reach 1 terabit/second due to their location above nearly all water vapor. Compared to free-space optical links, evidence suggests THz systems are superior where fog, cloud cover and clear-air turbulence are of concern.

Index Terms—Submillimeter wave communication, Satellite communication, Satellite ground stations, Submillimeter wave propagation

I. INTRODUCTION

IT is well known that the explosion of wireless communication has led to the demand for available bandwidth outstripping supply. Mobile and rural broadband networks are not only a major consumer of terrestrial bandwidth, but are now driving the demand for satellite capacity. Not only has this hindered the development of new and emerging networks, but has led to bandwidth being reallocated away from incumbent systems, especially satellite links and government users. It is against this background that carrier frequencies are being pushed from the microwave to the millimeter-wave and through the terahertz (THz) in order to exploit unused and previously inaccessible spectrum [1-4].

As frequencies increase, link losses from atmospheric attenuation, mainly from water vapor, dramatically increase. At the same time, available transmitter power decreases and

receiver noise increases. For this reason, it is commonly believed that spectrum from 100 GHz to 1 THz is only suited for short-range indoor communications. However, this application in itself has difficulties: scattering and reflection by building materials, furnishings and people are significant, and can severely impede non line-of-sight communication [5].

As both an alternate development path, and a means of realizing economies of scale, research into THz communication systems must explore alternate fields where there is already a proven demand for bandwidth, and is not severely cost, size or power sensitive.

The historical driving force behind THz technology has been radio astronomy, so it is not surprising that developments in this field have the potential to drive satellite communication. Specifically, large-aperture THz optics, both on the ground and in space have been developed and proven. At the forefront of these systems are the Atacama Large Millimeter/Submillimeter Array (ALMA) and the Herschel Space Observatory. Herschel observed in bands from 480 GHz through 5.3 THz with a 3.5-meter aperture. ALMA consists of fifty-four 12-meter and twelve 7-meter reflector elements located at an altitude of 4.8 km in Northern Chile.

We have previously modeled atmospheric attenuation, terrestrial and extraterrestrial noise sources, and the resulting integration time for various ground, airborne and spaceborne telescopes observing THz galaxies [6]. In a separate work, we analyzed the annual atmospheric precipitable water vapor (PWV) distribution over the entire surface of the Earth using high-resolution remote sensing satellite data and identified sites with the lowest water vapor [7]. This work identified specific dry locations, in addition to well-known astronomical sites, such as the Tibetan Plateau and high peaks in the Western United States, which have very low PWV values. For example, we found numerous dry locations with a median atmospheric attenuation of 20 dB at 667 GHz in the United States and Europe, located only hundreds of kilometers from locations with attenuation much in excess of 100 dB.

These works suggested an avenue for THz satellite communications. Just as in the case of radio astronomy, satellite ground terminals can be sited in locations that are locally dry in order to substantially reduce atmospheric attenuation. The proven technology of large-aperture ground and space THz optics can be utilized to create a highly directive link to mitigate the effects of remaining attenuation as well as immature THz source and detector technology. Additionally, airborne platforms, such as tethered aerostats and balloons, can fly above over 99% of all atmospheric water vapor, eliminating the majority of atmospheric attenuation.

We acknowledge support from the Center for Scientific Computing at the CNSI and MRL: an NSF MRSEC (DMR-1121053) and NSF CNS-0960316.

J. Y. Suen is with the Department of Electrical and Computer Engineering, University of California, Santa Barbara, CA 93106 USA (e-mail: jsuen@ece.ucsb.edu).

M.T. Fang, S. P. Denny, and P.M. Lubin are with the Department of Physics, University of California, Santa Barbara, CA 93106 USA.

Preprint Version, November 18, 2014.

There are many applications of these terabit-per-second point-to-point links, which are approximately ten times faster than current commercial microwave systems. The links can serve as backhaul for broadcast satellites, or for low earth orbit (LEO) satellite constellations. Beyond these traditional applications, the extreme data rate opens new scientific applications, such as space-based very large baseline interferometry (VLBI) arrays for radio astronomy. Here, extreme amounts of data, on the order of 20 terabytes per element per day, are generated and must be downlinked, though not necessarily in real time. There are security benefits: the narrow beam (less than 10 km) and the large apertures required makes interception and jamming difficult and easy to detect. For defense applications, an airborne link from a satellite to a high-altitude balloon or UAV can be covert and impossible to intercept or disrupt from the ground due to low-altitude atmospheric absorption.

The siting of ground terminals is critical for link performance but must also be balanced against infrastructure requirements. Antarctica, a common site for astronomy, is clearly infeasible. However, our analysis has identified many mid-latitude sites which both have reasonable THz link performance and infrastructure accessibility. For example, sites identified in the Western Continental United States offer reasonable access to fiber optic networks. Tanggula Station, Tibet, is a station along the Qinghai–Tibet railway. As the development of the ALMA telescope has shown, construction of electrical power and fiber optic infrastructure in the desolate Atacama Desert is feasible. Another option to be considered is the use of tethered aerostats, a proven technology, around major cities with moderate ground-level PWV.

In this paper, we combine a link budget and noise model with complete, global water vapor data and atmospheric modeling to show the feasibility of terabit per second satellite communication links both from low-PWV geographic locations as well as airborne platforms. We consider satellite-specific path geometry, modulation types, variable bandwidth, modeling of satellite terminals based on THz astronomical instruments and likely use cases. Specifically, we pattern the satellite off the THz optics of the Herschel space telescope, which we model in geostationary orbit. For the terrestrial terminals, we consider a variety of scenarios, from a single 12-m ground dish, based on the elements of the ALMA telescope, to a 1-meter aircraft antenna. Compared to our previous work, we utilized a different PWV dataset using microwave measurements, which provides all-weather sensing.

First, we discuss the microwave PWV data and atmospheric model used. Next, our link modeling methodology and assumptions are shown. The results of the model are presented, and finally, we compare the performance of our modeled geostationary satellite link to freespace optical links operating in the infrared.

II. MODELING

Figure 1 shows the major components and variables of our model. In this section, we discuss our remote sensing PWV data and atmospheric models. We then show our signal and noise modeling methodology, which factors in receiver noise

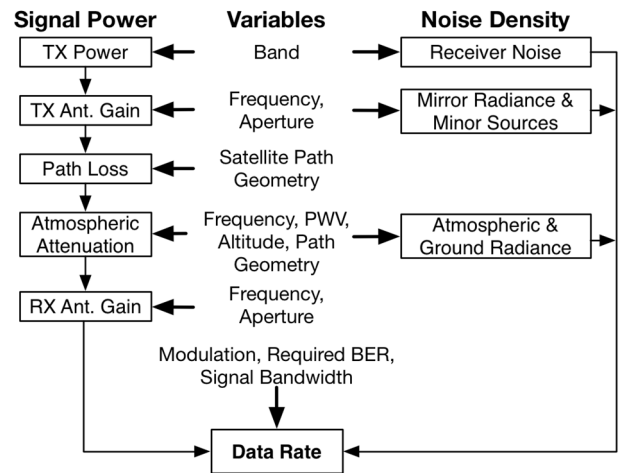


Fig. 1. Schematic of major model components and variables

and atmospheric radiance with antenna gain and path loss to calculate the maximum symbol rate. We next discuss the optimum modulation type and the optimum occupied bandwidth. Finally, we discuss how we derived the parameters of our modeled system, particularly receiver noise temperature and transmit powers.

A. Precipitable Water Vapor Maps

The primary source of atmospheric attenuation in the THz regime is absorption by water vapor due to its highly polar nature. Fortunately, water has a high freezing point and therefore a significant dependence of partial pressure on temperature. This effect causes water vapor to be concentrated at lower, warmer altitudes and locations. Water vapor is measured in terms of the precipitable water vapor (PWV), which represents the height of water if all of the water in a column of the atmosphere were condensed. The driest locations of the Earth have a median PWV of 0.1 mm while the wettest locations can exceed 60 mm. Because THz attenuation has a fundamentally exponential relationship to PWV, there are very significant geographical and seasonal variations in THz transmission.

In order to identify sites on a global basis, satellite remote sensing data must be used. The analysis and processing of our data was very similar to that of our previous work, using Matlab code written using a MapReduce parallel processing model [7]. As before, sun-synchronous satellites produced four PWV measurements per day, one in the morning and afternoon, repeating 12 hours later, over the entire surface of the Earth. Data for the entire 2012 calendar year was used. The fundamental difference in this work is that we chose to use PWV data based on microwave retrieval instead. We used the Microwave Integrated Retrieval System (MIRS) code from the NOAA Center for Satellite Applications and Research (STAR) [8] and processed the data from the AMSU-A and MHS microwave radiometers aboard the NOAA 18 and MetOp A satellites. The MIRS code was run in high-resolution mode, extrapolating the lower resolution AMSU-A data to produced data at the higher MHS resolution. The retrieval of the PWV by the MIRS code from the measured radiances took approximately 12,000 CPU core-hours and the processing of our model consumed an additional 5,000 core-hours.

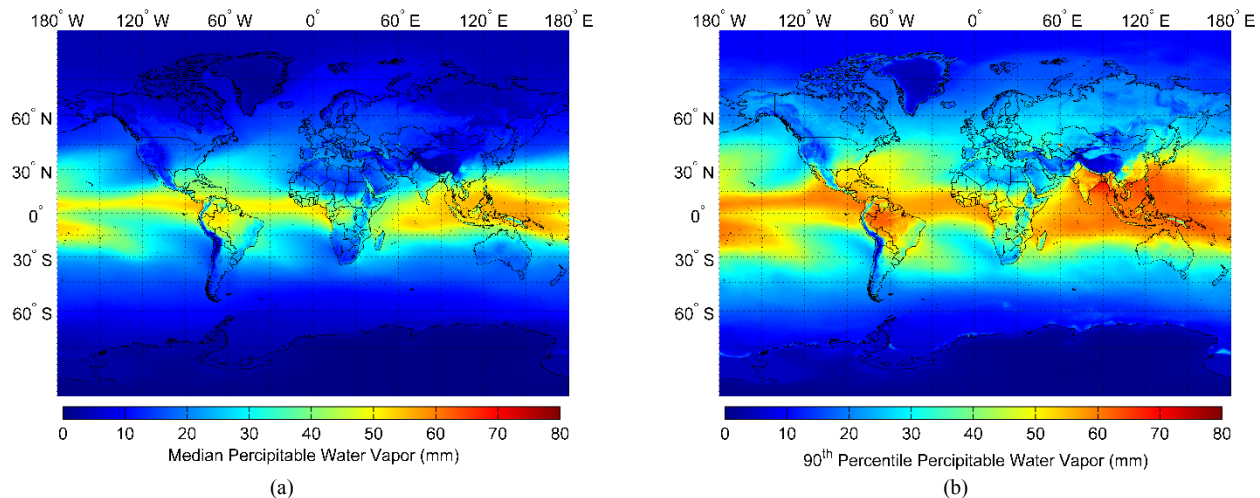


Fig. 2. (a) Median and (b) wettest 90th percentile all-weather PWV data used for locating ground sites. PWV was retrieved by MIRS code with NOAA 18 and MetOp A satellite data over the entire 2012 calendar year. High-resolution versions of the maps are available in the online supplemental materials.

Our previous dataset, based on infrared retrievals from the NASA Aqua and Terra satellites, could not retrieve PWV when the sky over a point was cloudy. Microwave sensing is able to sense water vapor through almost all sky conditions, with heavy rain being the exception. However, as a tradeoff, the resolution is lower, but still acceptable for this analysis. The previous and current datasets are not identical due to the different time period, sensing during cloudy weather, and resolution. Comparing dry sites, this data was slightly wet, which we account to the lower resolution.

The resulting PWV data was then gridded into pixels that were 0.2 degrees in longitude and latitude (22.24 km at the equator). There were an average of 1,364 valid PWV samples per gridded pixel. These included samples during active precipitation, which were, on average, 4.9% of the samples at a point. The statistics we present here are therefore all-weather. Figure 2 depicts our median and 90th percentile global PWV data set.

MIRS PWV data has been validated with a comprehensive study [9] and found to be accurate over all surfaces and all weather conditions except for rain. In the case of rain, the microwave radiometric signatures of liquid water and water vapor are difficult to distinguish. The data observed was within the intra-variability of the reference sources used. MIRS data was compared to National Centers for Environmental Prediction Global Data Assimilation System (GDAS) data, which is an assimilation system, using satellite, radiosonde and forecasts as inputs. PWV over land was found to have a correlation factor of 0.95 with a 0.73 mm wet bias for MIRS data. Compared to the NOAA radiosonde database for land measurements, a 0.92 correlation factor and a wet 2.00 mm bias was observed. The authors of the study note that it cannot be assumed that radiosonde measurements are automatically superior to satellite radiometry. The satellite data represents a true measurement to the top of atmosphere, while the radiosonde data used is truncated at 300 mb pressure. They note that the two measurements are not simultaneous in time or space and that there can be significant differences in the calibration and quality of the individual radiosondes. Comparison of MIRS data between two different

radiosonde data sets showed significant variability in the results.

To further examine the accuracy of the MIRS-retrieved PWV data in the low-PWV cases we are interested in, we compared radiosonde measurements at Nagqu, Tibet (median PWV 3.5 mm) to the MIRS-retrieved data over the same year. Since radiosonde data is taken at 12:00 and 24:00 UTC, the MIRS data is offset an average of 3.5 hours. For PWV points at 6 mm or less, the equation

$$PWV_{\text{Radiosonde}} = 0.9755 PWV_{\text{MIRS}} - 0.3355 \text{ mm} \quad (1)$$

related the two data sets with a root-mean-square error of 0.1424 mm. Thus, for the low-PWV case, the data correlates well, with MIRS data with a small wet offset, causing our predictions to be slightly conservative. The error increases for higher PWV values, which are likely associated with clouds and rain.

In both our studies, we utilized data spanning a full, single, calendar year. Analysis for the Cerro Chajnantor ALMA site has shown that while there can be significant interannual variation, austral winter variations are related to the El Niño Southern Oscillation (including El Niña) [10]. For the time period of 2011-2012 these events did not occur. The exact causes and magnitudes of variances are likely to be site-specific and require detailed study, but based on specific site measurements, we believe the data is broadly representative of a typical year.

Finally, retrieval of the PWV by the MIRS algorithm is dependent on the recognition of whether the point was over land or water. This caused small anomalies around bodies of water, particularly with the dry lakebeds of the Aral Sea. These points were not relevant to our study.

B. Atmospheric Modeling

For the atmospheric attenuation, we utilized the *am* version 7.2 atmospheric model [11]. We modified the *am* generic atmosphere profile. For ground sites, this assumed the path from space was to sea level. The generic atmosphere was truncated at the appropriate level for airborne systems. Since *am* was intended for radio astronomy and does not have a ground radiance model, we used radiance from the Modtran 5.2 code. We utilized a 3 GHz final frequency resolution,

matching the maximum resolution of Modtran. The attenuation data used from both models incorporated satellite geometry and used the appropriate zenith angles. No minimum elevation angle was assumed.

Usable THz spectrum is segmented into atmospheric windows, separated by strong absorption bands and narrow lines. The wide bands are caused primarily by water vapor, whereas gases, particularly oxygen, typically cause narrow lines. For the purposes of our analysis, we separate the THz spectrum into 6 bands, labeled A through F, ranging from 66 to 1,086 GHz (Table I).

We considered the effects of atmospheric scintillation and dispersion. A further discussion is given Section IV, where we compare scintillation in the THz bands to those in the optical regime. Scintillation in the THz bands is primarily caused by turbulence-driven variations in water vapor and manifests as changes in the amplitude and phase of the received signal. Dispersion is caused by the variation of attenuation across the bandwidth of the transmitted signals. Studies for large astronomical arrays, particularly the ALMA and the Combined Array for Research in Millimeter-Wave Astronomy (CARMA) instruments have found that the turbulent atmosphere at ground level causes the majority of scintillation. A single-antenna communication link is substantially unaffected by phase scintillation due to the high symbol rate. For any system, symbol times will be sub-nanosecond, far faster than any physical turbulence phenomena. As discussed in Section IV, there has been no direct characterization of the ground-space THz channel at relevant speeds, though measurements from ALMA suggest that deep fading is minimal.

A greater concern is the static variation of transmission across tens of GHz of bandwidth. As in microwave systems, multicarrier systems, such as orthogonal frequency division multiplexing (OFDM), are resistant to dispersion due to the smaller bandwidth of each individual carrier. Another method of compensating for this is with equalization, either digitally or with a physical filter. As in the case of scintillation, PWV variations in the THz path are slowly varying relative to the symbol rate, making the channel estimation problem easier.

In the case of astronomical arrays, water line radiometers have been well developed in to measure PWV and coupled with a model to compensate for phase and amplitude fluctuations over long integration times. Further, astronomical observations are usually radiometric, that is, measuring of the absolute source intensity, something not necessary in a communication system. Since we have control of the transmitted signal in a communications link, a separate instrument is not necessary as pilot tones or training sequences can be transmitted.

C. Signal and Noise Power Modeling

We calculated receiver performance in the matched filter limit, which assumes additive white Gaussian noise. We first determine the necessary symbol energy to noise density ratio, E_s/N_0 to sustain a desired bit error rate (BER). We considered typical modulations for wireless communication, specifically QPSK, 16-QAM, 64-QAM and 256-QAM signals. For QPSK,

$$\frac{E_s}{N_0} = (\text{erfc}^{-1}(2P_e))^2, \quad (2)$$

TABLE I
MODEL PARAMETERS

Parameter	Band/ Platform	Value	Remarks
Aperture Diameter	Ground	12.5 m	ALMA Telescope-class antenna
	6 km	3 m	Airship/Tethered Aerostat
	12 km	1 m	Aircraft
	18 km	1 m	High Altitude Balloon
	30 km	1 m	High Altitude Balloon
	Satellite	3.5 m	Herschel Telescope
Aperture Efficiency		0.7	
Carrier Bandwidth		3 GHz	For multicarrier signal
Pulse Shaping Filter		1.3	Bandwidth factor
Frequency Bands	A	66-186 GHz	
	B	186-327 GHz	
	C	327-555 GHz	
	D	567-747 GHz	
	E	759-984 GHz	
	F	996-1086 GHz	
Receiver Noise Temperature	Band A	1200° K	(DSB)
	Band B	3000° K	
	Band C-F	3600° K	
Transmitter Power Density (/3 GHz)	Band A	3 W	Bands A-B single
	Band B	1.25 W	TWTA per band
	Band C	175 mW	Bands C-F single
	Band D	100 mW	TWTA per carrier
	Band E	50 mW	
	Band F	10 mW	
Satellite Location		Geostationary at 118° W, 2° E, 122° E	
Desired Symbol energy-to-noise density ratio	QPSK	12.60 dB	Equivalent
	16-QAM	19.46 dB	BER=1 × 10 ⁻⁵
	64-QAM	25.57 dB	
	256-QAM	31.53 dB	

and for M -ary QAM,

$$\frac{E_s}{N_0} = \frac{2}{3(M-1)} \left(\text{erfc}^{-1} \left(\frac{2P_e M}{4(1-\sqrt{M})} \right) \right)^2, \quad (3)$$

where P_e is the BER. This rate was set to 10⁻⁵, which is the typical raw rate for many wireless communication systems. The resulting values are given in Table I.

The symbol energy, E_s , is the average received power divided by the symbol rate. The noise density $N_0 = kT_{sys}$, where k is Boltzmann's Constant and T_{sys} is the system noise temperature. Thus, the symbol rate,

$$R_{sym} = \frac{P_R}{K T_{sys}} \left(\frac{E_s}{N_0} \right)^{-1}. \quad (4)$$

The received signal power model simply used the Friis transmission equation, taking into account the satellite slant path distance. The system noise temperature is the sum of the noise temperatures from all sources. The majority of the noise comes from the receiver. Due to the high receiver noise contribution, and high carrier frequencies, the receiver is likely to be used in direct conversion mode, thus DSB noise temperature is used. Atmospheric and ground radiance make a minor contribution (~10%). Additionally, we accounted for all of the extraterrestrial noise sources and mirror emissivity from [6]. These contributed no more than 0.1% of the total noise power. The contribution from the uncooled reflector antenna is less than 1% of that of the atmosphere. Cooled optics are

unimportant for the THz communication, which may not be the case for carriers in the longwave IR.

D. Optimum Bandwidth Selection

When calculating the bandwidth necessary for a certain data rate, 1.3 Hz/symbol/second was used, which includes an additional 30% factor due to pulse shaping.

Due to the presence of narrow water and oxygen lines in the THz transmission spectra, the channel characteristics may vary significantly across each band. We considered two cases that span likely scenarios. First, we modeled the system using a single carrier, which is limited in overall data rate by the performance of the worst 3 GHz frequency bin occupied by the carrier. In the THz, narrow absorption lines will limit overall performance. This is also equivalent to a system that utilizes multiple contiguous carriers, all with the same modulation and symbol rate. With this constraint, we determined the contiguous frequency range to be utilized in order to maximize the overall data rate.

The second case, which we refer to as the multiple carrier case, utilizes multiple 3 GHz wide carriers, which may be realized by simply transmitting independent signals or via OFDM. The carriers share the same modulation type but

independently vary in data rate. By avoiding, this results in higher achievable data rate at the expense of system complexity. We present results from both cases.

E. Aperture and Transceiver Parameters

The aperture and transceiver parameters used in our model (Table I) are intended to match current technology as close as possible. The 3.5 meter satellite optics are patterned to match the Herschel Space Observatory [12] and the 12-m ground aperture matches a single element of the ALMA telescope [13].

We specified transmitter power (Table I) as a density, that is, a constant wattage for every 3 GHz occupied bandwidth. Within a single band, the total transmit power increases proportionally to bandwidth. This made comparison between the single carrier and multicarrier cases direct, and it represents the limited bandwidth of individual amplifiers.

Transmit power was based upon vacuum microelectronic devices, most developed under the DARPA High Frequency Integrated Vacuum Electronics (HiFIVE) and THz Electronics (THzE) programs. Since devices with 150 and 50 W of power have been demonstrated in Bands A and B, respectively [14, 15], we envision a system with one transmit amplifier per

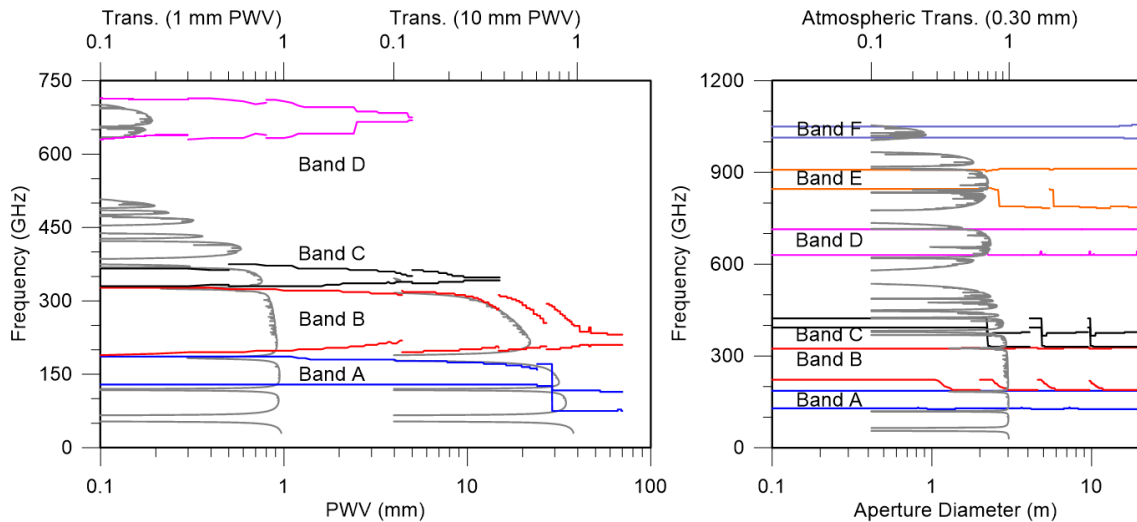


Fig. 3. Optimum single-carrier frequency as a function of PWV for a 45° latitude ground site (left) and a 6 km altitude airborne link (right). Also shown are atmospheric transmission spectra.

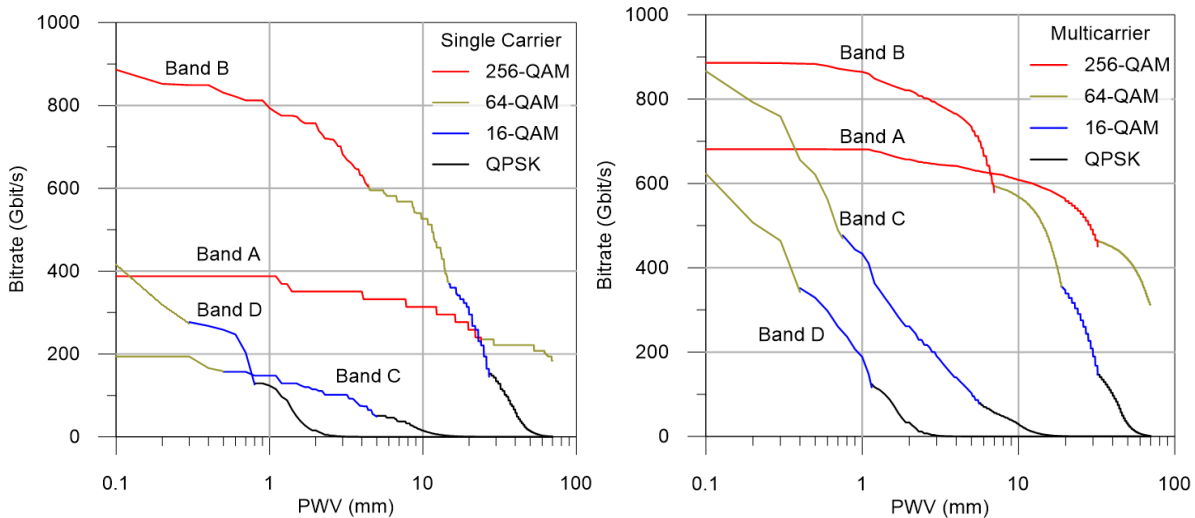


Fig. 4. 45° latitude ground site bitrate as a function of PWV for single-carrier (left) and multicarrier (right) systems.

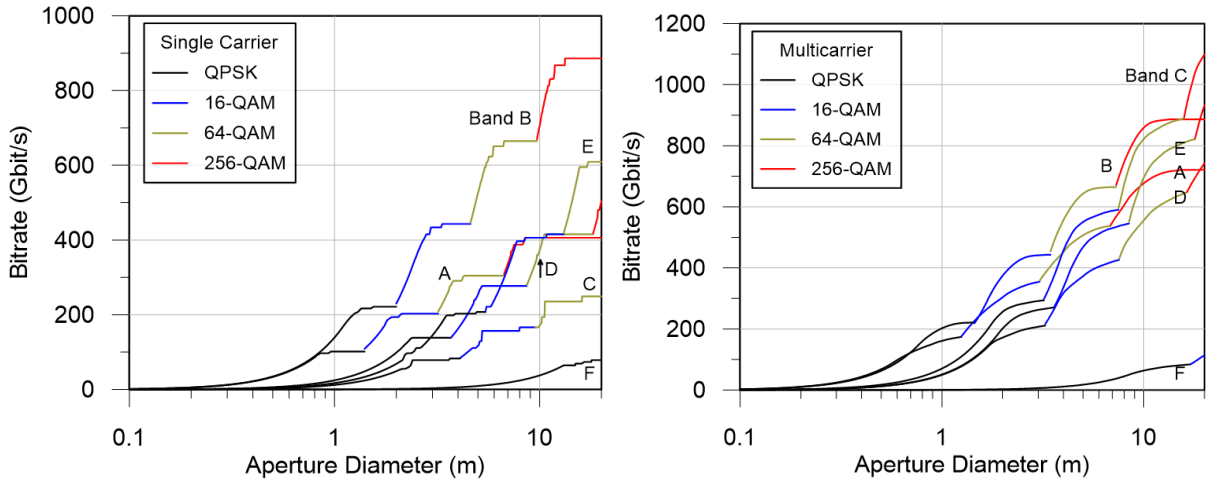


Fig. 5. 45° latitude 6 km airborne platform bitrate as a function of aperture diameter for single-carrier (left) and multicarrier (right) systems.

band. Bands C-E are enabled with compact amplifiers with outputs of 175, 100 and 50 mW [16-18], where the latter two have been demonstrated. Band F is based upon the THzE goal of 10 mW at 1030 GHz [19]. These are all compact devices, able to be held in one hand, so a system will use one device per 3 GHz, requiring 10-30 power modules.

Receiver noise performance matched commercial devices in all bands [20]. In the space segment, we modeled 3 satellites in typical geostationary orbital slots, separated by 120 degrees in longitude.

We also considered airborne Earth stations. These were an airship at 6 km altitude, an aircraft at 12 km, and balloons at 18 and 30 km altitude. Some applications envisioned for these platforms include an airship serving as either a metropolitan area wireless relay, or a tethered aerostat with a fiber-optic backhaul. Scientific applications include high-bandwidth data links for balloon-borne astronomical observations. In the defense domain, airborne platforms can utilize such high rate links for ultra-high resolution persistent surveillance or signals intelligence applications, while being impossible to detect or intercept. These platforms are above nearly all atmospheric water vapor and are minimally affected by clouds and rain.

The data we present models direct pointing between the satellite and terminal. Due to the large apertures and short wavelengths, beamwidths are extremely narrow, less than 0.1 degrees corresponding to footprints of less than 10 km. This fundamentally limits the system to a point-to-point link, though in practice, this does not preclude satellites with multiple apertures or steering of the apertures to form multiple links sequentially.

While the beamwidths are very small, both the ground and space systems we based our models upon have much finer pointing abilities. The ALMA array is designed to point to 0.6 arcseconds and the Herschel telescope 1.9 arcseconds, a fraction of the diffraction-limited beamwidth at our frequencies. Finally, the tracking of a geostationary link is greatly simplified as the satellite has very small apparent motion. It is much slower than the diurnal motion that telescopes must track and is far less than the tracking requirements for low earth orbit satellites. This eliminates a major engineering problem that has plagued LEO optical links.

III. RESULTS

In this section, we first discuss data rates for a generic site as a function of PWV or aperture size. We then show the performance over each band for ground sites and airborne scenarios. Finally, we find the data rate if all usable bands were combined, and discuss possible ground terminal sites.

A. Data rate versus PWV and Aperture Size

The primary variable that determines link performance for links to the ground is PWV. For airborne links, where PWV variations are minimal, aperture diameter, which is constrained based on the specific platform, is the primary variable. We examine the bandwidth and maximum bitrate as a function of these variables. Table II lists several representative link budgets showing the influence of each modeled component.

For both the single-carrier and multicarrier case, usable bandwidth is important as it influences the design of not only THz electronics but also of quasi-optical systems like feedhorns and combiners. Figure 3 shows the optimum single-carrier bandwidth for the ground case and for a 6 km altitude airborne terminal at mid-latitudes. Also shown are atmospheric transmission spectra showing the atmospheric absorption lines, which limit usable bandwidth. Sharp transitions in the bandwidth are points where modulation changes.

For the ground case, Band A shows unique behavior in that at low PWV, there is more usable bandwidth between the 183 GHz water line and the 118 GHz O₂ line. Above 30 mm PWV, the additional attenuation reduces the transmission such that the narrower region between the 60 and 118 GHz O₂ lines becomes optimal.

In the airborne 6 km case, available bandwidth differs significantly from the ground case due to the substantially reduced water vapor. Up to 380 GHz, the majority of the lines are due to oxygen. The usable portions of Bands A, B and the lower portion of Band C become nearly contiguous, except for the water line at 189 GHz and the oxygen lines at 330 and 380 GHz. The effects of water vapor still remain above 450 GHz, separating the bands into windows above this point. In band E,

TABLE II
TYPICAL LINK BUDGETS

	Ground Band B	Ground Band C	Ground Band C	12 km Band D	6 km Band E	18 km Band F
Parameter						
Center Frequency	225 GHz	350 GHz	350 GHz	675 GHz	875 GHz	1025 GHz
PWV	20 mm	5 mm	10 mm	0 mm	0.30 mm	0 mm
Link Power Budget (Per 3 GHz carrier)						
Transmit Power	31.0 dBm	22.4 dBm	22.4 dBm	20 dBm	17.0 dBm	10 dBm
Sat. Antenna Gain	76.7 dB	80.6 dB	80.6 dB	86.3 dB	88.6 dB	89.9 dB
Ground Ant. Gain	87.4 dB	91.3 dB	91.3 dB	75.4 dB	87.2 dB	79.1 dB
Path Loss	-231 dB	-235 dB	-235 dB	-241 dB	-243 dB	-244 dB
Atmospheric Transmission	-8.76 dB	-8.72 dB	-17.19 dB	-0.12 dB	-2.51 dB	-3.31 dB
Receive Power	-44.8 dBm	-49.4 dBm	-57.9 dBm	-59.1 dBm	-52.7 dBm	-68.7 dBm
Noise (Antenna Temperatures)						
Receiver Noise	3000 K	3600 K	3600 K	3600 K	3600 K	3600 K
Atmospheric and Ground Radiance	277.8 K	277.7 K	272.4 K	265.8 K	243.6 K	226.2 K
Other Sources	0.5 K	0.6 K	0.6 K	0.7 K	0.7 K	0.7 K
Rate						
Best Modulation	64-QAM	16-QAM	QPSK	QPSK	QPSK	QPSK
Min. Integration Time per Symbol at Center Freq.	491 ps	412 ps	595 ps	796 ps	182 ps	7.11 ns
Gbits/sec/GHz	4.07	3.08	1.12	0.838	1.53*	0.094
Max. Multicarrier	347 (16-QAM)	103	30.2	140	263	18.1
Bitrate over band						
Max. Single Carrier Bitrate over band	314 (16-QAM)	50.7 (QPSK)	15.7	69.0	144	8.31
Optimum Single Carrier Bandwidth	99 GHz	30 GHz	9 GHz	129 GHz	126 GHz	57 GHz

* Bandwidth Limited

Common Parameters: 3 GHz bandwidth, 45 degree latitude (51.8 degree zenith angle), site longitude equals satellite longitude

Other Noise Sources: Primary mirror radiance, Cosmic Microwave Background

the strong water vapor line at 910 GHz is limiting even up to large apertures.

Figure 4 depicts the maximum ground station link rate as a function of PWV, for both single carrier and multicarrier cases, and Figure 5 depicts the same for a 6 km platform. At many aperture sizes the link is bandwidth limited, shown as a flat portion on the curve. Aperture diameters centered in the flat regions should be avoided. While larger aperture sizes

yield better performance, the cost and weight of an antenna with diameter d generally scales as d^2 to d^3 . Optimizations of aperture sizes will not only help with size and weight, but the increase in beamwidth will also reduce the cost and complexity of the antenna pointing system.

B. Ground Site Performance

The performance of the satellite THz link to ground sites is

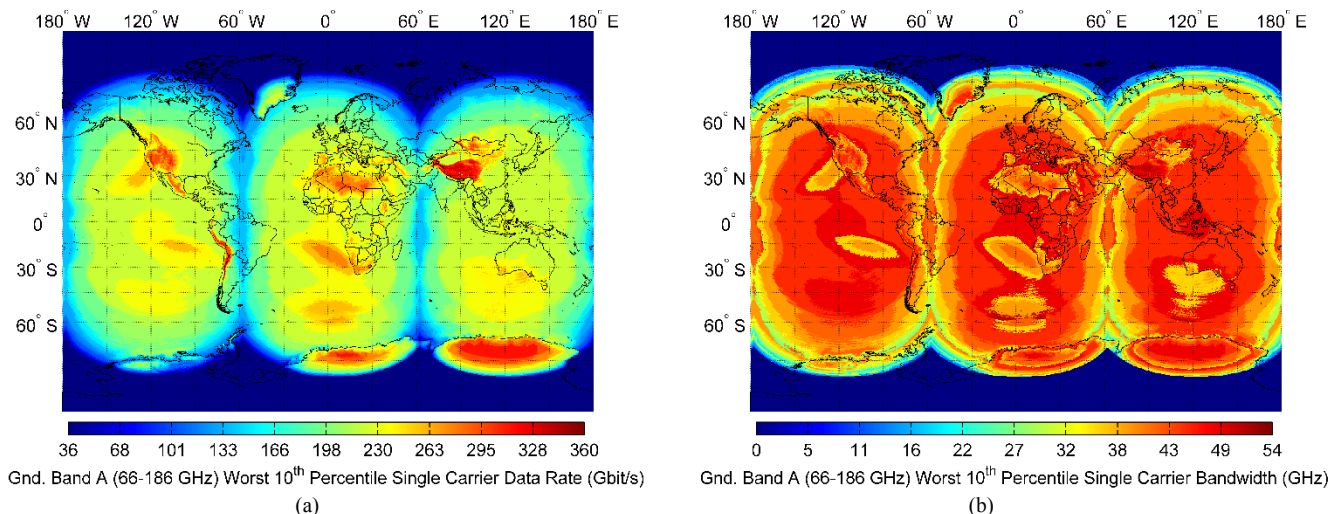


Fig. 6 (a) Band A data rate and (b) optimum usable bandwidth are shown. High-resolution versions of the maps are available in the online supplemental materials.

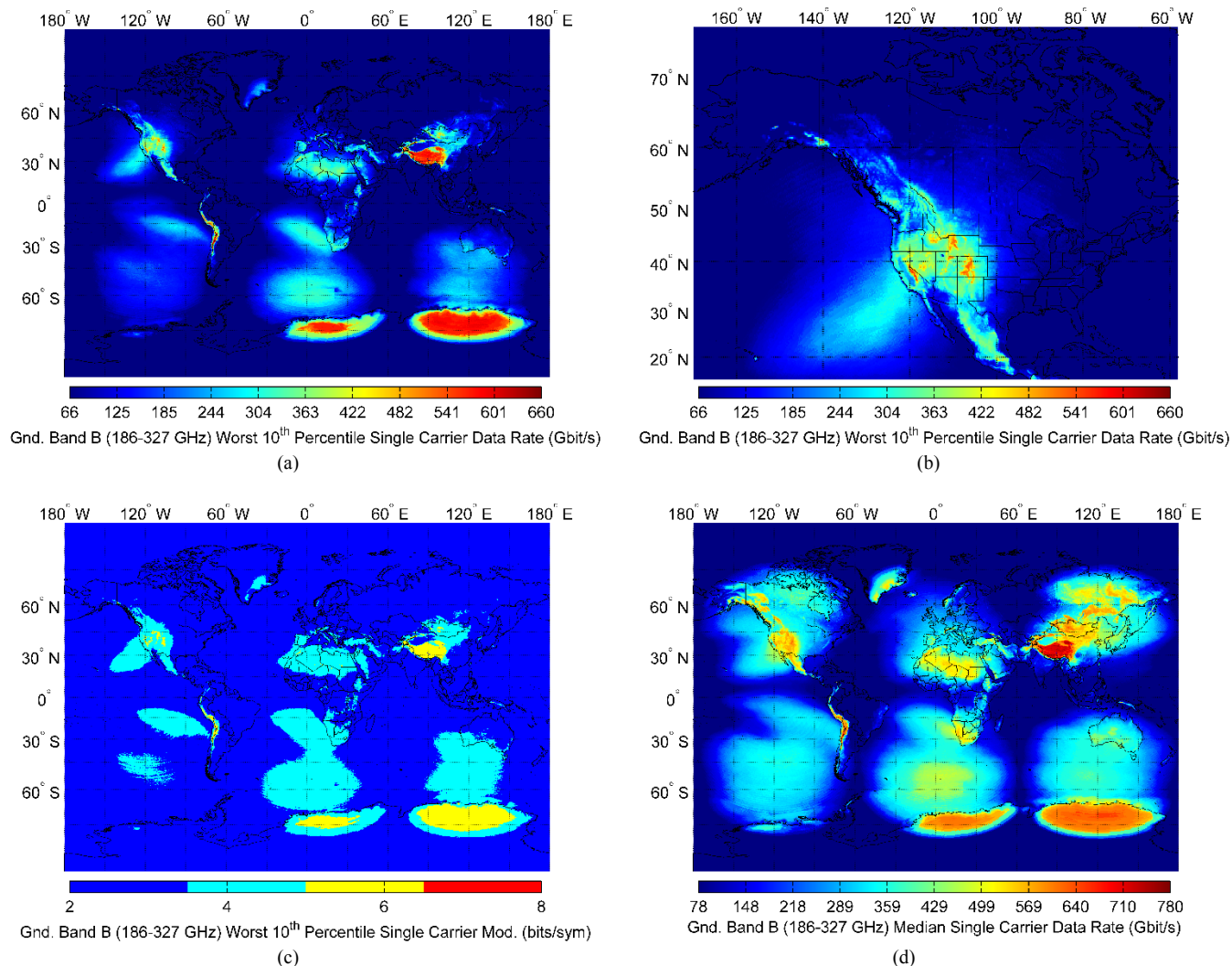


Fig. 7. (a) Band B data rate shown for the world, (b) and for North America. (c) optimum modulation, and (d) median statistics.

fundamentally limited by PWV, therefore we created maps combining the site-specific PWV and satellite path geometry. Typically, the driest sites, as used for astronomical observatories, operate in the 1-3 mm range, thus it is evident from our model that in Bands A through C, geostationary links operating at terabits per second are possible from these locations. However, most of the typical inhabited regions of the Earth range from 10-50 mm. For a geostationary link, only the sub-THz Band A will be universally available, though Band B has the potential to be usable at many sites.

The effects of the geographic variation of water vapor are immediately evident from the results. Figure 6a maps the worst 10th percentile Band A single-carrier data rate and indicates that even though the sub-THz band has comparatively low PWV sensitivity, data rates vary by around a factor of 2 within the main satellite footprint. Figure 6b shows the usable bandwidth for the same scenario and indicates that around 35-50 GHz of bandwidth is optimal, approximately half of the band. (High-resolution versions of these maps are available in the online supplemental materials)

Moving up to Band B (Fig. 7a), which operates between 183 and 321 GHz, the geographic dependence becomes even

more pronounced. There are large areas achieving 175 Gbit/sec, though moderately dry mid-latitude areas such as Western North America (Fig. 7b), Northern Africa and South Africa show performance around 350 Gbit/sec. The dry regions of the Andes and of the Tibetan Plateau have the best performance, in excess of 550 Gbit/sec. Figure 7c shows the modulation used. We note that this is for the worst 10th percentile, 256-QAM is necessary for many sites under median and better performance; refer to Fig. 4. Figure 7d shows the median rate, which is a good metric for systems which do not need a constantly available link, such as downlinking of science or remote sensing data which can be temporarily stored. Data rates are higher by a factor of 2-3, with 400 Gbit/sec data rates through areas such as Australia, China and Mongolia.

Centered around 350 GHz, Band C shows an extremely strong dependence on PWV. Performance in the worst 10th percentile is low, with typical dry regions reaching around 75 Gbit/sec. Due to the high data rate of Band B, this band will likely be used opportunistically. By sharing the same apertures, an additional link in this THz band can increase link throughput around 25% during the best 75% of the time.

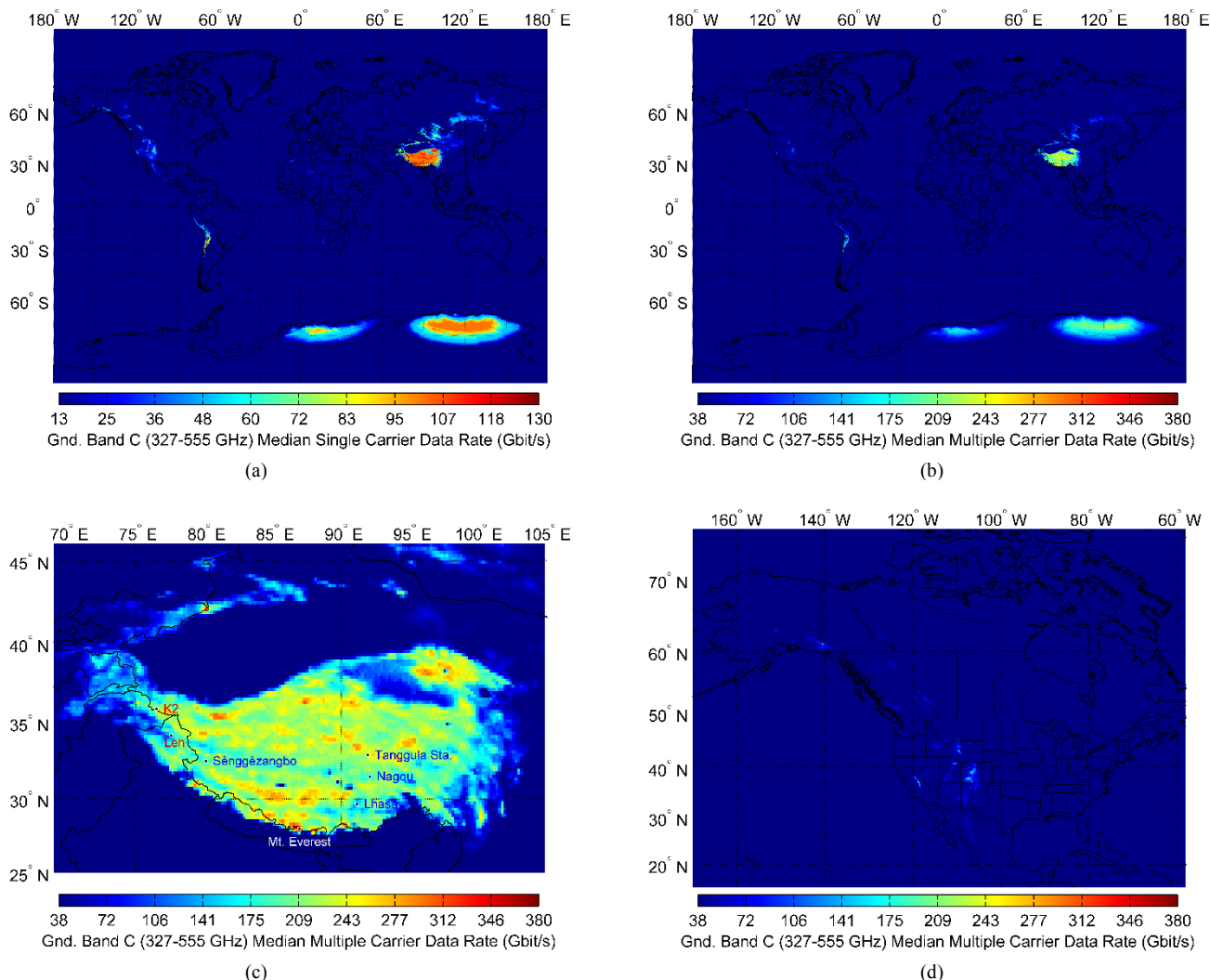


Fig. 8. (a) Median Band C data rate for the single carrier and (b) multicarrier model. (c) Detail views of Tibet and (d) North America are shown.

Figure 8a shows the global median data rates, showing that links only to globally dry sites are possible. In Band C there are numerous water lines, specifically there is an additional transmission window from 390-440 GHz in addition to the primary 325-380 GHz window. Figure 8b shows that in the multicarrier case, data rates are improved, though still geographically limited. Figure 8c and 8d are detail views of the median multicarrier link rate for Tibet and North America. These are the globally driest sites, aside from the Chilean Andes. Along with the Atacama Desert near the ALMA site, they are the most likely locations to develop a THz ground station.

C. Airborne Performance

Whereas atmospheric water vapor limits the performance from ground sites, aperture size is the dominant factor from airborne platforms. The relatively low scale height of water vapor, about 2 km, means that the 6 km altitude airship or aerostat scenario is above at least 95% of all atmospheric water vapor, increasing to 99% at 12 km. We do not consider the statistics or geographic distribution of water vapor as it is unlikely to vary significantly; the variation in rates seen is due to satellite path angle.

In many cases, a 3 m aperture at 6 km altitude outperforms a 1 m aperture at 30 km (Table III). In all but the 6 km altitude scenario, the SNR was inadequate to support more than QPSK modulation. Geographic coverage is limited by satellite path geometry.

Figure 9a shows the geographical distribution of single-carrier data rates with the 6 km airship (3 m aperture) model at Band E. The data rate variation is caused by satellite geometry. Figure 9b shows the same band with the 12 km (1 m aperture) aircraft scenario. The 38% lower peak data rate is due to the smaller aperture. Figure 9c shows the 18 km balloon-borne Band F scenario. Bitrates do not exceed 60 Gbit/sec. The multicarrier data rate, Figure 9d, shows a significant improvement, up to 130 Gbit/sec due to the continued influence of water lines, even at this altitude.

D. Band-Combined Performance

To fully maximize the value of ground and space segment infrastructure, multiple bands can be utilized simultaneously within a single aperture and link. Nearly all applications will require a bidirectional link, and thus systems will have to combine multiple frequencies, as well as transmitters and receivers together with one aperture.

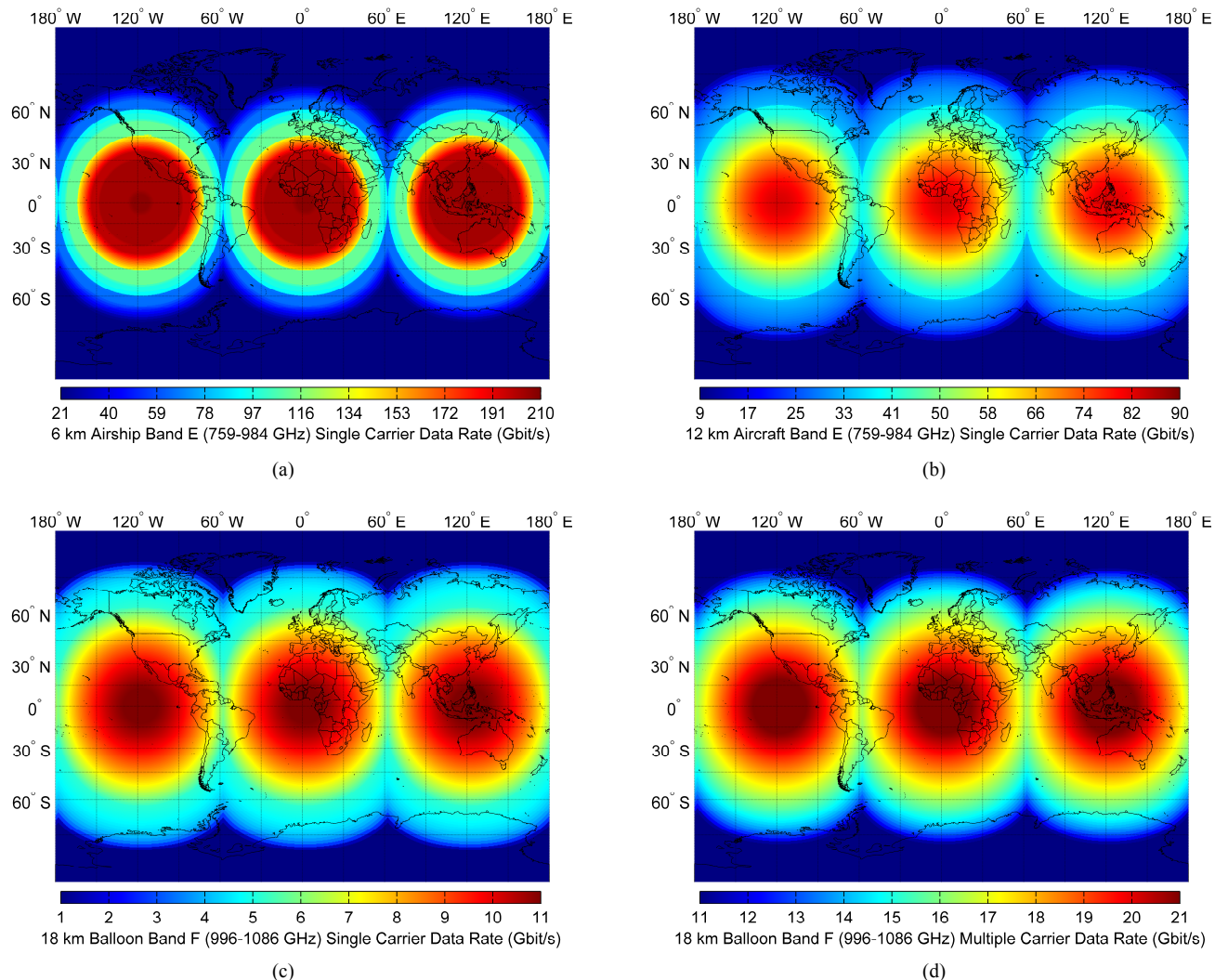


Fig. 9. Airborne scenarios at (a) 6 km, (b) 12 km and (c, d) 18 km altitudes are shown. Oxygen lines limit band F performance, as can be seen by the comparison of the 18 km single carrier (c) and multicarrier (d) cases.

TABLE III
MID-LATITUDE AIRBORNE DATA RATES (GBIT/S) AND MODULATION

Platform	Aperture Diameter	Band A (66-186 GHz)	Band B (186-327 GHz)	Band C (327-555 GHz)	Band D (567-747 GHz)	Band E (759-984 GHz)	Band F (996-1086 GHz)
Single Carrier							
6 km Airship	3 m	203	433	78	138	145	3.4
2 km Aircraft	1 m	101	147	48	70	55	5.7
18 km Balloon	1 m	102	147	48	71	55	8.4
30 km Balloon	1 m	131	147	85.9	107	111	11.7
Multicarrier							
6 km Airship	3 m	354	441	292	207	263	6.4
12 km Aircraft	1 m	163	207	145	142	150	17.4
18 km Balloon	1 m	166	207	148	144	157	18.3
30 km Balloon	1 m	169	207	155	151	162	19.2

Bold rates are 16-QAM, other rates are using QPSK modulation. Models a path from a satellite at 118° W to a point at 45° N, 118° W

There are a variety of methods such as time-division or frequency-division duplexing. The THz bands pose little challenge to these techniques, which have been well-developed in the microwave bands. Combining receivers and transmitters in different bands with waveguide duplexers can be done easily with high isolation and minimal loss. Assigning lower frequency bands for satellite downlink can be beneficial

due to the increased efficiency of transmitters on the power-constrained satellite. Quasi-optical circulators [21] and orthomode transducers have been designed for THz use, which can even allow for simultaneous uplink and downlink use of bandwidth. Therefore, the total link throughput, which is the sum of uplink and downlink throughput, will be between

approximately one and approaching two times the maximum unidirectional link rate.

Data rates for specific sites are summarized in Table IV. These sites were chosen to be representative of locations where a ground station could be located. The ALMA site represents an astronomical-quality location in the Chilean Andes. Despite its remote location, electrical power, road and fiber data infrastructure have already constructed. Tangula Railway Station, at 5 km altitude, is the highest station along the Qinghai-Tibet Railway and is drier than the ALMA site. Although the station is uninhabited and undeveloped, there is daily train service from Lhasa, the capital of the Tibet Autonomous Region. Fiber optics can be laid efficiently along the railroad suggesting that this site is very favorable not only due to low PWV but also in a price-performance comparison. Ali Shiquanhe, Tibet already hosts an astronomical observatory with road, power and data infrastructure. The Goldstone Deep Space Communications Complex represents a traditional microwave communications site which shows reasonable performance in Bands A and B, but not C.

We also locate several undeveloped sites. The High Uintas Wilderness site is located at an altitude of 3.1 km in the US state of Utah. It is about 30 km off a state highway and 100 km from the major metropolitan area of Salt Lake City. While the Matterhorn peak itself is inaccessible, significant tourist facilities, including cable cars are spread throughout the surrounding area, which is only about 100 km from Geneva. Tifouina, Morocco is located in the High Atlas mountain range has direct road access. Finally, Mt. Elbrus, Russia is located by the Russian-Georgian border. There has been access to this area by mountain climbing expeditions, a lower altitude site can be considered. These undeveloped sites have reasonable performance, including access to Band C greater than 90

TABLE IV
BAND-COMBINED (66-555 GHz) GROUND SITE PERFORMANCE

Site	Data Rate (Gigabits/sec)	
	Best Quartile/Median/Worst Quartile/Worst 10 th Percentile	
	Single Carrier	Multicarrier
ALMA Site, Chile 22.9° S, 67.9° W	1,149/1,081/978/894	1,640/1,557/1,427/1,221
Tanggula Sta., Tibet 32.9° N, 91.9° E	1,298/1,200/1,021/960	1,932/1,721/1,527/1,357
Ali Shiquanhe, Tibet 32.3° N, 80.0° E	1,182/1,108/960/854	1,709/1,598/1,347/1,189
Goldstone, USA 35.5° N, 116.9° W	932/854/743/563	1,269/1,217/1,142/915
High Uintas Wilderness, USA 40.7° N, 110.5° W	1,194/1,079/937/853	1,699/1,562/1,276/1,201
Matterhorn Region, Switzerland 45.9° N, 7.7° E	1,155/1,015/894/811	1,650/1,518/1,238/1,163
Tifouina, Morocco 31.9° N, 6.1° W	1,146/997/924/852	1,619/1,435/1,264/1,207
Mt Elbrus, Russia 43.3° N, 42.5° E	1,096/978/837/667	1,574/1,366/1,154/1,059

percent of the time.

Figure 10 presents maps of the combined link performance. Figures 10a and 10b depict the worst 10th percentile performance, single and multicarrier respectively. In both cases, data rates over 1 Tbit/sec are possible from dry locations. For median rates (Figs. 10c and 10d), many mid-latitude sites can support this rate.

For the 6 km airship scenario, the mid-latitude combined rate exceeds 1 terabit per second when combining six single carriers covering bands A-F (Fig. 10e) and exceeds 1.8 terabits per second in the multicarrier case (Fig. 10f). As previously discussed, the limiting factor in the airborne cases is receive aperture size; the 3 m dish is necessary for terabit per second performance.

Often applications require a minimum data rate be sustained with a very high availability, in excess of the 90% we presented. The uplink for a satellite television broadcast system is an example. Any kind of radio communication system is subject to disruption by environmental conditions; heavy snow and rain are well-known problems, even for microwave links. In order to counter these events, and to maximize the minimum guaranteed data rate, multiple sites may be used to mitigate regional conditions. Not only can we avoid local weather events, but also exploit differences in seasonality between Northern and Southern hemisphere locations. A satellite can simply be re-pointed to the best site and if the system utilizes in-orbit crosslinks, the sites can even be located in the footprints of different satellites.

Ideally, these redundant sites should be located such that the link rate of the best site at any instant is as close to the global maximum as possible. Of course, there is a cost-benefit tradeoff with the number of redundant sites. Under these constraints, it may be beneficial to trade off peak rate for overall availability. Optimizing the placement of multiple sites requires further large-scale data analysis and optimization and is an avenue for future study. Additionally if we are interested in reliability over very short timescales, local weather patterns must be analyzed over these timescales, which may be down to hours or minutes, as is in the case that “5 nines” (99.999%) availability is necessary.

IV. COMPARISON TO OPTICAL LINKS

The THz satellite communications link modeled in this paper shares many similarities with optical ground-to-satellite links [22]. These links operate in the infrared at wavelengths around 800 or 1550 nm. A primary driver of these wavelengths is the availability of compact and low-cost sources, amplifiers, and detectors, which can operate both at high powers and speed. The proposed applications are similar in that they serve as a point-to-point link either as backhaul for a backbone or access layer, or for downlink of high-rate data from scientific or other sensing satellites. Both utilize very high carrier frequencies to allow high-bandwidth communications. A full model of the IR optical channel is beyond the scope of this paper, but we make a general comparison of the two technologies.

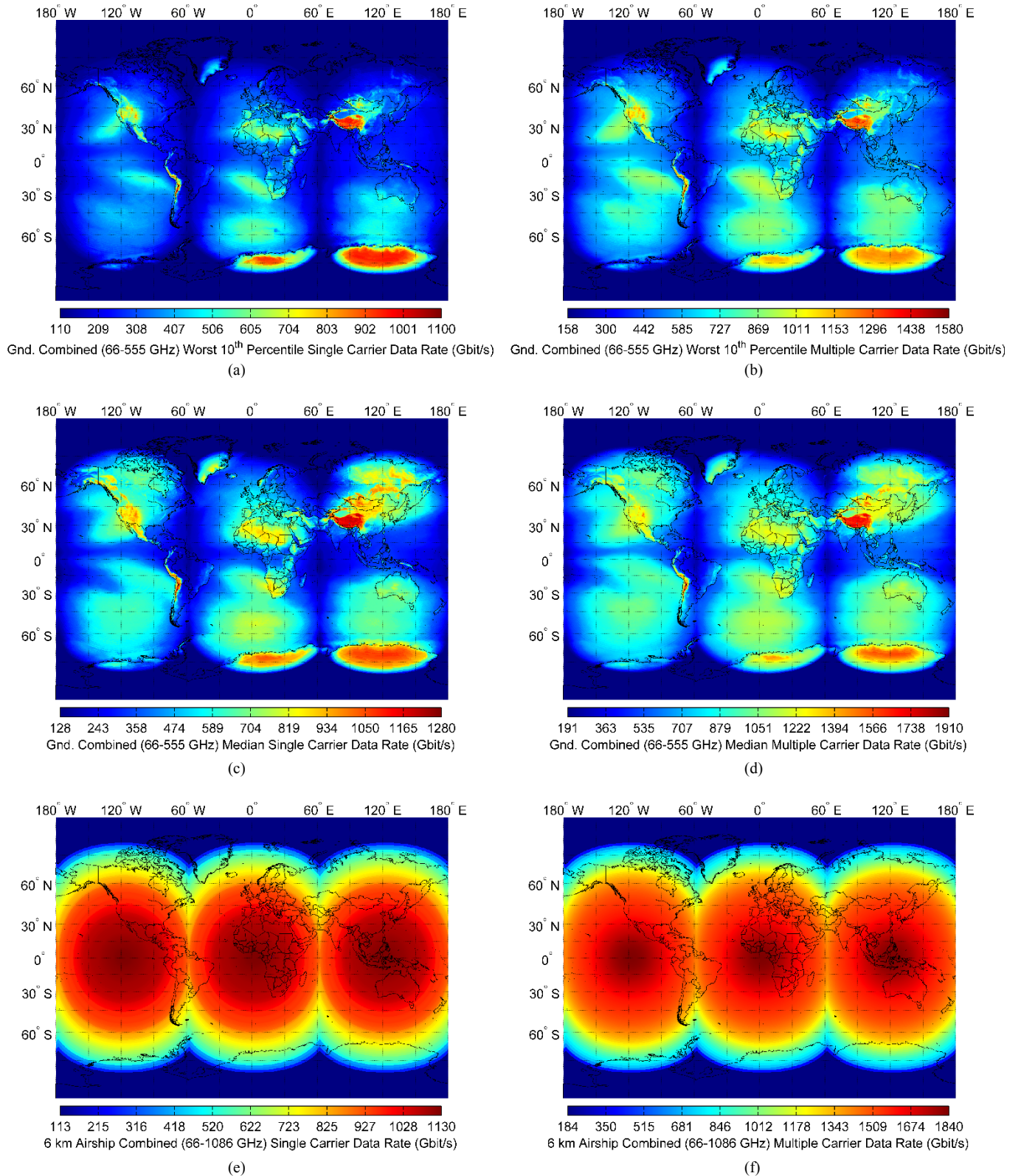


Fig. 10. Data rates achieved by combining multiple bands. Ground scenarios (a-d) utilize bands A-C, while the 6 km airship scenario (e, f) utilizes bands A-F. Both single carrier (a, c, e) and multicarrier (b, d, f) scenarios are shown, as well as worst 10th percentile (a, b) and median (c, d) rates.

In both the THz and IR, systems are fundamentally limited by atmospheric effects. The 800 and 1550 nm bands are atmospheric windows which, like the THz, are defined by water vapor absorption. Both systems utilize apertures

thousands of wavelengths across in order to form tightly collimated beams. Table V shows the link budget effects of scaling the carrier from 650 GHz to 1550 nm using measured aperture gain, transmission and path loss data from an

experimental low earth orbit (LEO) satellite link in [23]. Of note is the poor link reliability observed with this satellite with only 15 of 32 link attempts successful in the reference. 16% of link attempts failed due to clouds, whereas there was a failure to acquire the satellite 22% of the time. While acquisition and tracking is more difficult due to the motion of a LEO satellite, failure due to clouds or excess atmospheric turbulence is of concern.

A significant difference between the optical and THz regimes is the availability of high power optical sources and the maturity of infrared receiver technology. Direct detection devices can operate at tens of photons per bit, while coherent detectors can offer performance that is limited by source quantum noise (BLIP limit) [24]. However, this does not, in itself, imply a dramatic improvement over the THz receivers we modeled. First we note that while kilowatt-class fiber amplifiers exist, any ground link will have to conform to eye safety limits.

Let us assume a perfectly efficient and noiseless photon-counting detector operating at 1.55 μm with negligible background. If we assume a binary modulation (1 bit/photon, such as on-off keying or binary pulse-position modulation, PPM) operating at 100 gigabits/second, the necessary received power is bounded by

$$P_r \geq MR \frac{hc}{\lambda} = -48.9 \text{ dBm}, \quad (5)$$

where M is the modulation order (bits/symbol), R is the bit rate, h is Planck's constant, c the speed of light, and λ the carrier wavelength. Under these idealized conditions we see that the necessary photon-limited receive power is within 20 dB of our THz cases. Increasing modulation order to 256-PPM results in a 9 dB decrease in necessary power, but adding a more realistic 10 photons/symbol detector efficiency results in a 10 dB increase in receiver input power. While a full analysis and comparison of photon-counting receivers and modulation is beyond the scope of this paper (reference [22] discusses limits of photon-counting channels), we believe that a realistic IR communication system will have a link budget within 20-30 dB of the THz systems modeled here.

Atmospheric turbulence is a factor in both communications systems, whereby variations in the effective path length result in fluctuations in signal intensity. This scintillation is caused by constructive and destructive interference due to propagation over differing paths. The exact mechanism through which this occurs varies. In the IR, this is mainly due to changes in the refractive index of air, which has a temperature and pressure dependence. High-altitude clear-air turbulence is the primary source of this scintillation, but it can also be caused by boundary-layer turbulence if a terminal is carried aboard an aircraft. A comparative analysis of this effect in [1] indicates that the changes in optical path length are approximately equal in the IR and THz regimes and thus scintillation effects scale should scale inversely with the carrier wavelength.

In contrast, changes in water vapor concentration along the propagation path are a more significant effect in the THz bands, due to both the significant in-band attenuation of water vapor and high refractive index. This PWV variation is also driven by atmospheric turbulence, but due to the non-uniform mixing of water vapor, it occurs at the atmospheric boundary

TABLE V
COMPARISON OF THZ AND 1550 NM LINK LOSS

	Ground Band C (5 mm PWV)	12 km Band D	Ground 1550 nm
Sat. Ant. Gain	80.6 dB	86.3 dB	113 dB
Ground Ant. Gain	91.3 dB	75.4 dB	113 dB
Atmospheric Trans.	-8.72 dB	-0.12 dB	-2.01 dB
Path Loss	-235 dB	-241 dB	-289 dB
Total	-71.8 dB	-79.4 dB	-65.0 dB
Difference from IR	-6.8 dB	-21.2 dB	

Band C and D: 45 degree latitude path

1550 nm parameters: 25 cm apertures, 0.7 aperture efficiency. Atmospheric loss is measured averages of ground to low earth orbit link from [16]. Pointing error loss (-1.17 dB) and Scintillation (-4.44 dB) reported in [16] are conservatively assumed to be equal over all bands due to lack of data in the THz case. Path loss is to geostationary orbit.

layer (extending from the ground up 1-2 km). Although there has been comprehensive work on the effects of clear-air turbulence on IR communication links, there has been limited study of this phenomenon in the THz. Most existing work concerns the effects of phase variations over physically large multi-aperture arrays, such as the ALMA telescope (up to 16 km baselines), and over long (>1 s) integration times [25]. This is of little concern in a single-aperture communication receiver, especially since differential phase-shift keying only requires a phase coherency time on the order of several symbol periods. For high-bandwidth systems, the sub-nanosecond symbol period far exceeds the speed of physical atmospheric phenomena. Further, phase-reference pilot tones can be transmitted, a technique similar to the use, in astronomical observations, of a guide star.

Rather, the primary concern with scintillation in a THz communications system is not the overall phase variance but the amplitude variance, caused by interference between phase variations within the wavefront received by a single aperture. In the IR, fades of around 5 dB can be expected to occur at rates of greater than 100 Hz with fade lengths scales in excess of 100 μs [26]. For THz, the effects are still largely unknown. Characterization of PWV variance over short surface paths have shown that the variance in humidity approximately follows a Kolmogorov form, indicating clear-air turbulence models, modified for the vertical distribution of water vapor, are also applicable in the THz. Modeling of the effects at 650 GHz with this moderately-humid low-altitude PWV data, has shown transmission variance of around 1-10% over a 100 m ground path [27]. Observations from astronomical arrays such as ALMA and CARMA confirm that most of the PWV variation is due to low-level turbulence. These amplitude variations are no more than several percent in the highest frequency bands, thus we believe that any deep fading to be minimal and on small time scales.

Both IR and THz links are affected by clouds, fog and dust. The attenuation of IR radiation through these aerosols is well characterized and is severe. As in the visible range, loss through fog and clouds are primarily due to scattering. These water droplets are in the 1-20 μm range, close to the optical carrier wavelength, and thus exhibit strong Mie scattering. While water vapor is highly attenuating in the THz regime, absorption bands of liquid water is significantly narrower. Measurements of propagation through aerosols show relatively little impact in the THz range. Experimental

measurements of THz and 1550 nm propagation through intense dust show negligible THz attenuation when compared to IR [28]. Modeling and simulation of cloud attenuation has shown that, for a mid-latitude site with 20-30% cloud cover, the 99th percentile worst attenuation is less than 4 dB at 100 GHz and 10 dB at 300 GHz, and the 90th percentile attenuation is better than 1.5 and 3 dB, respectively. [29] We conclude that, unlike in the IR, the effects of cloud cover are minimal at THz frequencies.

Rain will have a greater effect on the THz bands than at IR as the droplet sizes are closer to the carrier wavelength, though heavy rain is far less prevalent than clouds, especially at low PWV locations. Experimental measurements have shown that, even in the rainy climate of Japan, attenuation will be less than 4 dB at 120 GHz over 99.9% of a year [30].

Overall, both THz and IR satellite communication links both serve similar applications and share many similar characteristics. The clear-sky link budget is comparable between the two regimes, with the THz link showing about 7 dB more loss from the ground. The main benefits of an IR link are smaller apertures. This is valuable in airborne links, which are aperture size constrained in the THz cases. Here, the IR model shows a link budget advantage of 21 dB over THz. For high velocity aircraft platforms, the IR advantage will be significantly reduced by boundary layer turbulence and increased pointing error losses that we do not account for. However the, IR link still shows superiority for high-altitude balloons.

In contrast, the THz bands are far superior where clouds and aerosols are of concern, particularly for links to the ground and low-altitude airships. It is foreseeable that ground-based high-bandwidth links will have a greater commercial demand than airborne links, while being intolerant to cloud outages. We believe that the development of THz satellite communication links is technically competitive with IR links and are an important avenue to satisfy the demand for bandwidth.

V. CONCLUSIONS

We have shown that even with severe atmospheric attenuation in the THz bands, very high bitrate geostationary satellite links are possible, exceeding 1 terabit per second from both ground and airborne platforms. Large-aperture space and ground THz optics are already in use for radio astronomical observations, which has also led to the development of infrastructure in very dry locations. Development in high-power THz sources is also a key enabling technology. Even though significant work is necessary to test and commercialize a THz satellite link, it is clear that any new satellite earth stations must be future-proofed for both THz and IR optical links by the analysis and on-site measurements of PWV, ground-level turbulence, rain and cloud cover rates. The global analysis of high-resolution all-weather PWV levels by satellite remote sensing is important in identifying these regions.

Our model shows that 256-QAM modulation is necessary for bands up to 327 GHz, and 16-QAM for almost all scenarios. The phase stability and amplitude linearity of sources, modulators, and receivers are therefore important.

THz satellite links share many similar characteristics to optical links operating in the infrared. They both use a strong directional beam for very high bitrate communications. The advantages of infrared systems are much smaller apertures, due to the shorter wavelength, though the overall propagation loss is comparable. The major advantage of THz that it is resistant to cloud and fog scattering, a significant problem in optical systems. Further, the effects of scintillation, caused by atmospheric turbulence and, when operating from aircraft, boundary-layer turbulence, should be several orders of magnitude less in the THz than in the optical domain. These characteristics suggest that THz links will have better availability than IR systems.

In conclusion, as radio astronomical observatories have demonstrated, strong atmospheric water vapor absorption of THz radiation is not an insurmountable obstacle to long-distance THz communication, but instead with large-aperture antenna technology and careful site planning, use of THz bands can be an important means of satisfying the explosive demand for communications bandwidth.

REFERENCES

- [1] J. Federici, and L. Moeller, "Review of terahertz and subterahertz wireless communications," *J. Appl. Phys.*, vol. 107, no. 11, pp. 111101, Jun. 2010.
- [2] E. R. Brown, "Fundamentals of Terrestrial Millimeter-Wave and THz Remote Sensing," in *Terahertz Sensing Technology, Vol. 2: Emerging Scientific Applications and Novel Device Concepts*. Singapore: World. Sci., 2004, pp 93-196.
- [3] S. Koenig, D. Lopez-Diaz, J. Antes, "Wireless sub-THz communication system with high data rate," *Nature Photonics*, vol. 7, pp 977-981, Oct. 2013.
- [4] H-J. Song, T. Nagatsuma, "Present and Future of Terahertz Communications," *IEEE Trans. THz Sci. Tech.*, vol. 1, no. 1, pp 256-263, Sep. 2011.
- [5] R. Piesiewicz, C. Jansen, D. Mittleman *et al.*, "Scattering Analysis for the Modeling of THz Communication Systems," *IEEE Trans. Antennas Propag.*, vol. 55, no. 11, pp 3002-3009, Nov. 2007.
- [6] S. P. Denny, J. Y. Suen, and P. M. Lubin, "Fundamental Limits of Detection in the Far Infrared," *New Astron.*, vol. 25, pp 114-129, Dec., 2013.
- [7] J. Y. Suen, M. T. Fang, and P. M. Lubin, "Global Distribution of Water Vapor and Cloud Cover—Sites for High-Performance THz Applications," *IEEE Trans. THz Sci. Tech.*, vol. 4, no. 1, pp 86-100, Jan. 2014.
- [8] S-A Boukabara, K. Garrett, W. Chen *et al.*, "MiRS: An All-Weather IDVAR Satellite Data Assimilation and Retrieval System," *IEEE Trans. Geosci. Remote Sens.*, vol. 49, no. 9, pp 3249-3272, Sep. 2011.
- [9] S-A Boukabara, K. Garrett, W. Chen, "Global Coverage of Total Precipitable Water Using a Microwave Variational Algorithm," *IEEE Trans. Geosci. Remote Sens.*, vol. 48, no. 10, pp 3608-3621, Oct. 2010.
- [10] R. Bustos, G. Delgado, L.-A. Nyman, *et al.*, "52 Years of Climatological Data for the Chajnantor Area," NRAO, Charlottesville, VA, Rep. 333, 2000.
- [11] S. Paine, "The am atmospheric model," *Smithsonian Astrophys. Obs.*, Cambridge, MA, Rep. 152, Ver. 7.2, 2012.
- [12] P. R. Roelfsema, F. P. Helmich, D. Teyssier *et al.*, "In-orbit performance of *Herschel*-HIFI," *Astron. Astrophys.*, vol. 537, no. A17, Dec. 2011.
- [13] A. Lungren, "ALMA Cycle 2 Technical Handbook," ver. 1.1, ALMA, Santiago, Chile, 2013, pp 115.
- [14] A. J. Theiss, C. J. Meadows, R. Freeman, *et al.*, "High-Average-Power W-band TWT Development," *IEEE Trans. Plasma Sci.*, vol. 38, no. 6, pp 1239-1243, Jun. 2010
- [15] K. E. Kreischer, J. C. Tucek, M. A. Basten, *et al.*, "220 GHz Power Amplifier Testing at Northrop Grumman," in *2013 IEEE 14th International Vacuum Electronics Conference (IVEC)*, Paris, 2013, pp. 1-2.
- [16] J. H. Booske, W. J. Lee, S. Gallagher, *et al.*, "Microfabricated TWTs as High Power, Wideband Sources of THz Radiation," in *The 9th International Conference on Terahertz Electronics*, Charlottesville, VA, 2001.
- [17] J. C. Tucek, M. A. Basten, D. A. Gallagher, *et al.*, "A 100 mw, 0.670 THz Power Module," in *2012 IEEE Thirteenth International Vacuum Electronics Conference*, Monterey, CA, 2012, pp. 31-32.

- [18] J. C. Tucek, M. A. Basten, D. A. Gallagher, *et al.*, "0.850 THz Vacuum Electronic Power Amplifier," in *IEEE International Vacuum Electronics Conference*, Monterey, CA, 2014, pp. 153-154.
- [19] J. D. Albrecht, M. J. Rosker, H. B. Wallace, *et al.*, "THz Electronics Projects at DARPA: Transistors, TMICs, and Amplifiers," in *2010 IEEE MTT-S International Microwave Symposium Digest (MTT)*, Anaheim, CA, 2010, pp. 1118-1121.
- [20] Virginia Didoes. (2013, Dec. 1). Available: <http://vadiodes.com>
- [21] R. I. Hunter, D. A. Robertson, P. Goy, *et al.*, "Design of High-Performance Millimeter Wave and Sub-Millimeter Wave Quasi-Optical Isolators and Circulators," *IEEE Trans. Microw. Theory Tech.*, vol. 55, no. 5, pp. 890-898, May 2007.
- [22] V. W. S. Chan, "Free-Space Optical Communications," *J. Lightwave Technol.*, vol. 24, no. 12, pp 4750-4762, Dec. 2006.
- [23] M. Toyoshima, S. Yamakawa, T. Yamawaki *et al.*, "Long-Term Statistics of Laser Beam Propagation in an Optical Ground-to-Geostationary Satellite Communications Link," *IEEE Trans. Antennas Propag.*, vol. 53, no. 2, pp 842-850, Feb. 2005.
- [24] V. W. S. Chan, "Optical Space Communications," *IEEE J. Sel. Topics. Quantum Electron.*, vol. 6, no. 6, pp 959-975, Nov. 2000.
- [25] B. Nikolic, R. C. Bolton, S. F. Graves *et al.*, "Phase correction for ALMA with 183 GHz water vapour radiometers," *Astron. Astrophys.*, vol. 552, no. A104, Apr. 2013.
- [26] H. T. Yura, and W. G. Mckinley, "Optical scintillation statistics for IR ground-to-space laser communication systems," *Appl. Opt.*, vol. 22, no. 21, pp 3353-3358, Nov. 1983.
- [27] S. G. O'Brien, D. H. Tofsted, "Terahertz Target Illumination Fluctuation Estimates Derived from Field Measurements of Atmospheric Water Vapor," *Proc. SPIE*, vol. 6949, no. 694906, May 2008.
- [28] K. Su, L. Moeller, R. B. Barat *et al.*, "Experimental comparison of terahertz and infrared data signal attenuation in dust clouds," *J. Opt. Soc. Am. A*, vol. 29, no. 11, pp 2360-2366, Nov. 2012.
- [29] G. A. Siles, J. M. Riera, P. García-del-Pino *et al.*, "Considerations on cloud attenuation at 100 and 300 GHz for propagation measurements within the TeraSense Project," in *Proc. 5th European Conf. Antennas and Propagation*, Rome, 2011, pp. 90-94.
- [30] A. Hirata, R. Yamaguchi, H. Takahashi, *et al.*, "Effect of Rain Attenuation for a 10-Gb/s 120-GHz-Band Millimeter-Wave Wireless Link," *IEEE Trans. Microw. Theory Tech.*, vol. 57, no. 12, pp. 3099-3105, Dec. 2009.



Jonathan Y. Suen (SM'03) received an A.A. degree from Bard College at Simon's Rock in 2002, the B.S. degree from the University of California, Santa Barbara in 2004, and the M.S. degree from the University of Michigan, Ann Arbor in 2005, all in Electrical Engineering. He recently received his Ph.D. in 2014 at the University of California, Santa Barbara in the Department of Electrical and Computer Engineering.

His research centers on the development of terahertz systems and has published research on biomedical imaging, THz sources and components, as well as systems for astrophysical observations and THz communications. He was the founder of an Internet startup and currently.



Michael T. Fang is currently an undergraduate student pursuing a B.S. degree in Physics and Mathematical Sciences at the University of California, Santa Barbara.

He has been an undergraduate researcher for the UCSB Experimental Cosmology group in the Department of Physics since late 2011 and has been conducting research on millimeter-wave and terahertz astrophysics.

Sean P. Denny Biography unavailable at time of submission



Philip M. Lubin received the Ph.D. degree in Physics from the University of California, Berkeley, in 1980.

Since 1987 he has been a Professor at the University of California, Santa Barbara. His research centers on millimeter-wave studies of the Cosmic Microwave Background (CMB). He is involved with the COBE and Planck cosmology satellites as well as leading the development of ground- and balloon-borne instruments. His research also includes work on THz and infrared detectors and systems.

Prof. Lubin was a co-recipient of the Gruber Prize in Cosmology in 2007 for his work on the Cosmic Background Explorer (COBE) satellite mission on ground-breaking studies of the CMB.